Polymer Vol. 39 No. 23, pp. 5839–5851, 1998
0032-3861/98/$ – see front matter

PII: S0032-3861(98)00084-6

Structural and relaxation studies during crystallization of New TPI polyimide

Srivatsan Srinivas† and Garth L. Wilkes*
Department of Chemical Engineering and Polymer Materials and Interfaces Laboratory, Virginia Tech, Blacksburg, VA 24061, USA
(Received 3 February 1997; revised 15 January 1998; accepted 21 January 1998)

The morphological development during crystallization and its subsequent effect on the relaxation behaviour for a series of cold-crystallized samples of a commercial polyimide, Mitsui Toatsu's New TPI, has been studied. Small angle X-ray scattering (SAXS) results showed that both the average lamellar and amorphous layer thicknesses increased with increasing crystallization temperature; the degree of crystallinity was also shown to increase with increasing crystallization temperature by wide angle X-ray scattering (WAXS). The glass transition temperature, however, was shown to decrease with increasing crystallization temperature. Increasing crystallization time at a given crystallization temperature produced an increase in T_g, with the increase following a log time dependence. An interesting feature observed from the dynamic mechanical studies was that for low crystallization times, the dependence of T_g on crystallization time was different from that for higher crystallization times, the changeover time corresponding to spherulitic impingement. The degree of crystallinity was shown to increase with increasing crystallization time; at low crystallization times, a prominent increase was observed due to a primary crystallization process, following which a further gradual increase in crystallinity was observed, corresponding to a secondary crystallization process. This was accompanied by a decrease in the average lamellar thickness; the average amorphous layer thickness, however, remained unchanged. This has been explained on the basis of a secondary crystallization process leading to the formation of thinner lamellae in the amorphous regions between different lamellar stacks, which gives rise to the lower melting endotherm (T_c + 10) observed in d.s.c. scans.

(Keywords: New TPI; crystallization; relaxation behaviour)

INTRODUCTION

Recent interest in the development of polymeric materials for use in engineering applications has led to extensive research in the area of high-temperature/high-performance polymers. Perhaps the most important category of high-performance thermoplastic polymers are the aromatic polyimide-based systems. These polymers, if of reasonable molecular weight, are tough, rigid and thermo-oxidatively stable polymers which possess excellent mechanical properties, as well as chemical and radiation resistance. These properties have made them suitable for use in a variety of engineering applications, such as in electrical and electronic applications, aerospace applications, adhesives, and as composite matrix materials[1–4]. The increasing importance of this polymer system has resulted in a variety of studies on polyimides by various research groups including our own[5–21].

A recent commercially available crystallizable polyimide is Mitsui Toatsu's 'New TPI', which has been the subject of considerable study over the past few years[9,22–32]. New TPI, the structure of which is shown in *Figure 1*, is based on pyromellitic dianhydride (PMDA) and 3,3′-bis(4-amino-phenoxy) biphenyl diamine (BAPB). The structure shows the presence of flexible ether linkages and meta substituted phenyl groups, resulting in an observed glass transition of *ca*. 250°C and an observed melting temperature of 385°C. This system exhibits good thermal stability as evidenced by the high values of 2% weight loss temperatures (545°C) in air as well as nitrogen, by t.g.a. studies[9]. Earlier work from our laboratory addressed the effect of thermal history on the subsequent crystallization and melting behaviour of New TPI, which showed that the loss of crystallizability of the polyimide with increasing melt time/temperature was caused by a drop in the nucleation density as well as chemical changes occurring in the material[9].

Crystalline samples of New TPI have been shown to exhibit a stacked lamellar morphology as shown by small angle X-ray scattering (SAXS) studies[22,23,25,27] arranged in a spherulitic superstructure; negatively birefringent spherulites with characteristic Maltese cross patterns were observed by Hsiao *et al*.[22]. Isothermal crystallization kinetic studies were carried out by Hsiao *et al*.[22], Cebe *et al*.[25], and Maffezzoli *et al*.[28] and analysed using the Avrami approach. Hsiao *et al*.[22] observed that isothermal crystallization from the melt occurred with an Avrami exponent of 4, whereas, in contrast, Maffezzoli *et al*.[28] reported Avrami exponents of 2 during isothermal crystallization from the melt. Isothermal crystallization from the glass yielded Avrami exponents ranging from 2.8 to 3.5, depending on the crystallization temperature[25].

The effect of crystallization time and temperature on the crystallization, melting and relaxation behaviour of a series of cold-crystallized samples of Aurum™ New TPI has been investigated in this study. The crystallization and melting behaviour have been studied utilizing differential scanning

* To whom correspondence should be addressed
† Present address Exxon Chemical Company, Baytown Polymer Center, Baytown, TX, USA

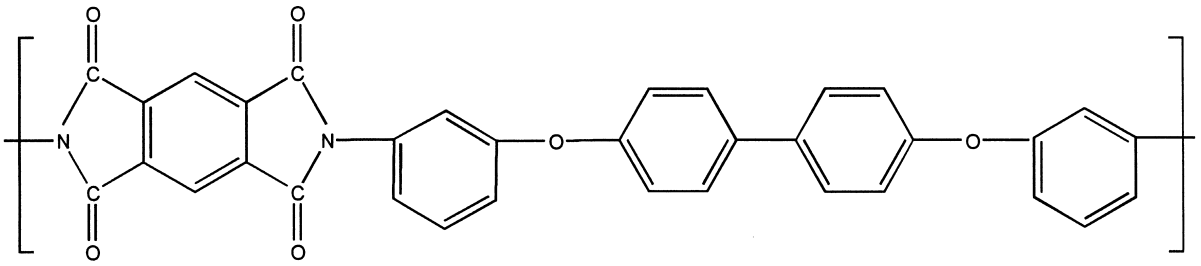

Figure 1 Chemical structure of New TPI

calorimetry (d.s.c.) in conjunction with wide angle X-ray scattering (WAXS). Structural changes occurring in the polymer have been investigated using SAXS in conjunction with dynamic mechanical analysis (DMS). By combining our results, along with previous work in this area, we hope to present a more comprehensive picture of the changes accompanying the crystallization process in New TPI.

EXPERIMENTAL

Sample preparation

The New TPI used in this study was in the form of amorphous extruded film. All samples were sandwiched between Teflon sheets and annealed at 265°C for 10 min in a preheated hot press in order to remove any orientational/residual stresses in the film which may have arisen as a result of processing. No pressure was applied while the platens of the hot press were kept in contact with the samples. No shrinkage of the films was observed after this annealing step, indicating no appreciable orientation in the as-received films. After the annealing step, the films were crystallized at different temperatures for various times in a hot press that was already maintained at the required temperature. Again, no pressure was applied to the samples. At the end of the crystallization step, the hot press was switched off and the samples allowed to cool slowly below T_g.

Characterization techniques

D.s.c. experiments were carried out on a Perkin Elmer DSC 7, under a nitrogen purge, using heating rates of 10°C min^{-1}. Temperature and heat flow were calibrated using indium and zinc as the standards. The weight of all samples were kept as consistent as possible (*ca*. 9.5 mg). The d.s.c. traces shown here have been normalized to a 1 mg sample mass.

Dynamic mechanical experiments were carried out on a Seiko DMS 210 under a nitrogen purge. The heating rate used in all experiments was 1°C min^{-1}. Sample lengths of 10 mm and cross-section area of *ca*. 0.3 mm^2 were tested at frequencies ranging from 0.01 Hz to 20 Hz.

SAXS experiments were performed on a Kratky camera using Ni filtered CuK_α radiation ($\lambda = 1.54$ Å) and equipped with an M Braun position sensitive detector. The methods used for the data analysis are described along with the results.

WAXS experiments were conducted on a Nicolet diffractometer equipped with a STOE Bragg–Brentano-type goniometer. CuK_α radiation of wavelength 1.54 Å was used after monochromatization through a graphite monochromator. Data were collected at 0.05° increments at angles between 5 and 70°. The theory and methods used to analyse the WAXS data are also described along with the results.

RESULTS AND DISCUSSION

WAXS studies

The determination of the degree of crystallinity in polymers using WAXS relies on the ability to deconvolute the scattering occurring due to the crystalline and amorphous regions from the total scattering. The crystalline fraction in a polymer is, therefore, the ratio of the integrated scattering arising from the crystalline domains to the total integrated scattering arising from the entire sample.

The degree of crystallinity can, hence, be determined by the following equation[33]

$$X_c = \frac{\int_0^\infty s^2 I_c(s)\mathrm{d}s}{\int_0^\infty s^2 I(s)\mathrm{d}s} \tag{1}$$

where s is the angular variable defined as $2\sin\theta/\lambda$, where 2θ is the radial scattering angle, $I_c(s)$ is the scattering intensity originating from the crystalline fraction, and $I(s)$ is the total scattered intensity from the sample.

The above equation underestimates the degree of crystallinity because part of the scattering from the crystalline regions does not contribute to the crystalline peaks, but appears as diffuse scattering, thereby contributing to the amorphous scattering. This diffuse scattering contribution from the crystalline regions is due to two reasons: atomic thermal vibrations and lattice imperfections. The methods most commonly used to determine the degree of crystallinity do not take into account the diffuse scattering from the crystalline regions (e.g. the Hermans and Weidinger method). Perhaps the only method that takes into account the diffuse scattering arising from thermal vibrations and lattice imperfections, is the method due to Ruland[34,35]. This method takes into account the loss of intensity of the crystalline peaks due to all departures of the lattice motifs (atoms or molecules or segments of molecules) from their ideal positions, by including a lattice imperfection factor in the intensity expression.

Taking the lattice imperfection factor into account, the degree of crystallinity X_c can be written as

$$X_c = \frac{\int_0^\infty s^2 I_c(s)\,\mathrm{d}s}{\int_0^\infty s^2 I(s)\,\mathrm{d}s} \frac{\int_0^\infty s^2 \bar{f}^2\,\mathrm{d}s}{\int_0^\infty s^2 \bar{f} D\,\mathrm{d}s} \tag{2}$$

where D is the lattice imperfection factor, where $D = \exp(-ks^2)$ and k is a term from different types of defect structure. The term $\bar{f}^2$ is given by

$$\bar{f}^2 = \frac{\sum N_i f_i^2}{\sum N_i} \tag{3}$$

and is the mean-square atomic scattering factor of the polymer.

Table 1 Degree of crystallinity from WAXS measurements for samples isothermally cold-crystallized for 135 min at various temperatures

Crystallization temperature (°C)	Degree of crystallinity (%)
280	17
290	22
300	24
310	26
320	26

Based on the above equations, the degree of crystallinity of an isotropic semicrystalline polymer of known chemistry can be estimated. In this study, the degree of crystallinity of the various samples were estimated using the method described by Ruland, and which has also been described and used by Vonk[36], our implementation of which will be described elsewhere[37].

The degree of crystallinity values for samples isothermally cold-crystallized for 135 min at various temperatures estimated using the Ruland method are given in *Table 1*. It can be seen that the degree of crystallinity increases by *ca*. 9% on increasing the crystallization temperature from 280°C to 320°C. However, the samples crystallized at 310°C and 320°C displayed essentially identical crystallinities.

The degree of crystallinity dependence on crystallization time for samples crystallized at 300°C is shown in *Figure 2*. The sample crystallized for 2.2 min at 300°C showed the presence of a small amount of crystallinity; samples crystallized for 6 min and higher, however, showed the presence of a substantially greater fraction of crystallinity. The degree of crystallinity increases rapidly to a value of *ca*. 23%, in the first 15 min; for longer times, the degree of crystallinity shows a gradual increase with the log of crystallization time, and increases to a value of *ca*. 28% at *ca*. 7000 min. Isothermal cold-crystallization experiments showed the primary crystallization process to be complete within 15 min at this temperature. The further increase in the degree of crystallinity with time after 15 min can, therefore, be attributed to a secondary crystallization process, which causes the formation of new lamellae accompanied perhaps by perfection of the existing lamellae. The morphological changes accompanying secondary crystallization and the subsequent effect on the amorphous phase is discussed in the following sections. Based on the Avrami analysis of isothermal cold-crystallization, Cebe *et al*.[25] had hypothesized that the development of crystallinity in New TPI takes place mostly during primary crystallization, and had suggested the absence of a secondary crystallization process. Based on the results presented in *Figure 2*, however, it seems clear that a substantial fraction of crystallinity during isothermal cold-crystallization develops as a result of secondary crystallization.

D.s.c. studies

Systematic studies of the crystallization and melting behaviour of New TPI under isothermal and non-isothermal conditions have been carried out by Cebe *et al*.[23,25]. The effect of crystallization time and temperature on the melting behaviour and glass transition of New TPI has also been discussed by Cebe *et al*.[25]. We will, therefore, not attempt to present all details of our d.s.c. studies, but present some results as they pertain to our dynamic mechanical and SAXS data.

Figure 3 shows the d.s.c. traces of amorphous New TPI, a sample crystallized at 300°C for 2.2 min, and a sample crystallized at 300°C for 135 min. Similar to the amorphous sample, the sample crystallized at 300°C for 2.2 min displays a prominent T_g, followed by a crystallization exotherm and finally by a melting endotherm. However, it can be seen in the figure that the temperature and area under the crystallization exotherm of the sample crystallized for 2.2 min is lower than that of the amorphous sample, clearly implying that some crystallization had occurred as a result of residence at 300°C for 2.2 min. From a calculation of the areas under the crystallization exotherm and the melting endotherm, we concluded that the amorphous sample was essentially amorphous before the d.s.c. scan, whereas the sample crystallized for 2.2 min had a small degree of crystallinity (*ca*. 6%), based on $\Delta H_f^\circ = 139\ J\ g^{-1}$, which is consistent with the WAXS results discussed earlier which yielded a value of *ca*. 6%. It should be recognized that, in calculating the degree of crystallinity by d.s.c., we implicitly assume that the enthalpy of melting and crystallization are independent of temperature. The sample crystallized at 300°C for 135 min displayed a weak T_g, followed by a small melting endotherm at 315°C, followed by a prominent melting endotherm at 385°C.

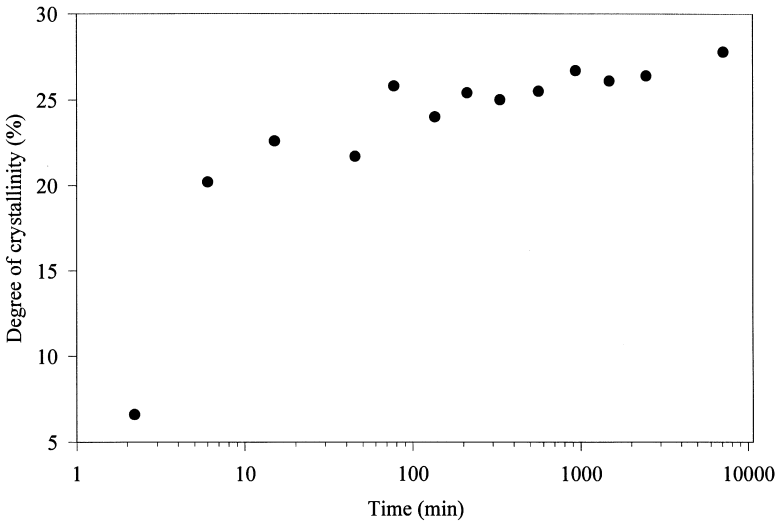

Figure 2 Degree of crystallinity as a function of crystallization time at 300°C

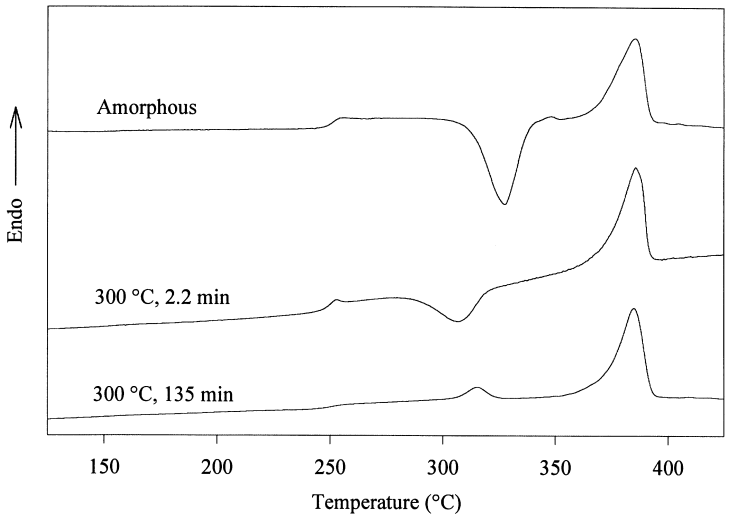

Figure 3 D.s.c. traces of amorphous and semicrystalline samples of New TPI

Most semicrystalline polymers exhibit multiple melting endotherms when crystallized/annealed at temperatures between T_g and T_m[9,38–43]. The lower melting endotherm is usually observed at temperatures 10–20°C above the crystallization temperature. Though there is considerable controversy in the literature regarding the origin of the low endotherm, evidence favours the explanation that the low endotherm corresponds to the melting of thin crystals formed as the result of a secondary crystallization process, following the formation of the dominant lamellae; the melting of the dominant lamellae is believed to give rise to the higher melting endotherm in the d.s.c. scan, the position of which is relatively insensitive to crystallization conditions. All samples studied here except the amorphous sample, the sample crystallized at 300°C for 2.2 min, and the sample crystallized at 300°C for 6 min, displayed a double endothermic behaviour in the d.s.c. scan; while the sample crystallized for 15 min exhibited a weak ($T_c + 10$°C) endotherm, the samples crystallized for longer times exhibited prominent low endothermic behaviour in the d.s.c. scans. From isothermal cold-crystallization studies, it was observed that the primary crystallization process was complete within 15 min; the WAXS results shown in *Figure 2* also indicate that the primary crystallization process was complete within 15 min. This supports the view that the low endotherm in the d.s.c. scan corresponds to the lamellae formed as a result of secondary crystallization.

The glass transition temperature was estimated from the mid-point of the specific heat transition accompanying the glass transition. *Figure 4a* shows the glass transition temperatures of samples crystallized for 135 min at various temperatures. The glass transition temperature was found to decrease with increasing crystallization temperature; possible causes for this observed behaviour will be discussed in the later section concerning the dynamic mechanical studies. The decrease in T_g on increasing the crystallization temperature from 280°C to 320°C was *ca*. 3°C, which is consistent with the findings by dynamic mechanical analysis. An important difference between the d.s.c. results and the dynamic mechanical results, however, is that the T_g (determined from d.s.c.) of the sample crystallized at 280°C was shifted by only *ca*. 2°C relative to the fully amorphous sample, a shift much smaller than that reported for cold-crystallized samples of other stiff chain polymers like PEEK[39] and PPS[40]. The dynamic mechanical results, however, showed that the sample crystallized at 280°C displayed a T_g (determined from the tan δ peak) that was *ca*. 10°C above a representative amorphous sample (crystallized at 300°C, 2.2 min).

The samples crystallized at 300°C or higher seemed to display a d.s.c. T_g that was lower than that of the fully amorphous sample. Such behaviour was also reported by Cebe *et al*.[25] from their d.s.c. studies. This is probably the result of the considerable broadening of the glass transition region and reduction in the specific heat jump at T_g due to the presence of crystallinity, thus introducing some uncertainties in the determination of the T_g from the mid-point of the specific heat jump at the glass transition.

The position of the lower melting endotherm was found to increase with increasing crystallization temperature, which is consistent with the $T_c + 10$°C behaviour of this endotherm; the upper melting endotherm was, however, independent of crystallization temperature in the range of temperatures studied here. It is to be expected that the melting temperature would, in general, increase with increasing crystallization temperature. However, under conditions of high undercooling, such as those employed in this study, the observed melting temperature of polymers is typically independent of crystallization temperature[25,39,40].

The d.s.c. glass transition temperature is shown as a function of crystallization time at 300°C in *Figure 4b*. It can be seen that the T_g increases with crystallization time, which, again, is consistent with the results of the dynamic mechanical studies discussed later. For the case of samples crystallized for lower times, the T_g appeared to be lower than that of the fully amorphous polymer. At higher crystallization times, the T_g increased above that of a fully amorphous sample, showing a log time dependence, similar to the dependence of crystallinity in the later stages of crystallization, as shown in *Figure 2*.

The position and area of the upper melting endotherm were found to be essentially independent of crystallization time. The peak position and area of the lower melting endotherm were, however, found to increase monotonically with the log of crystallization time, which is consistent with earlier reports on the behaviour of the low endotherm[25,43], and is also consistent with the log

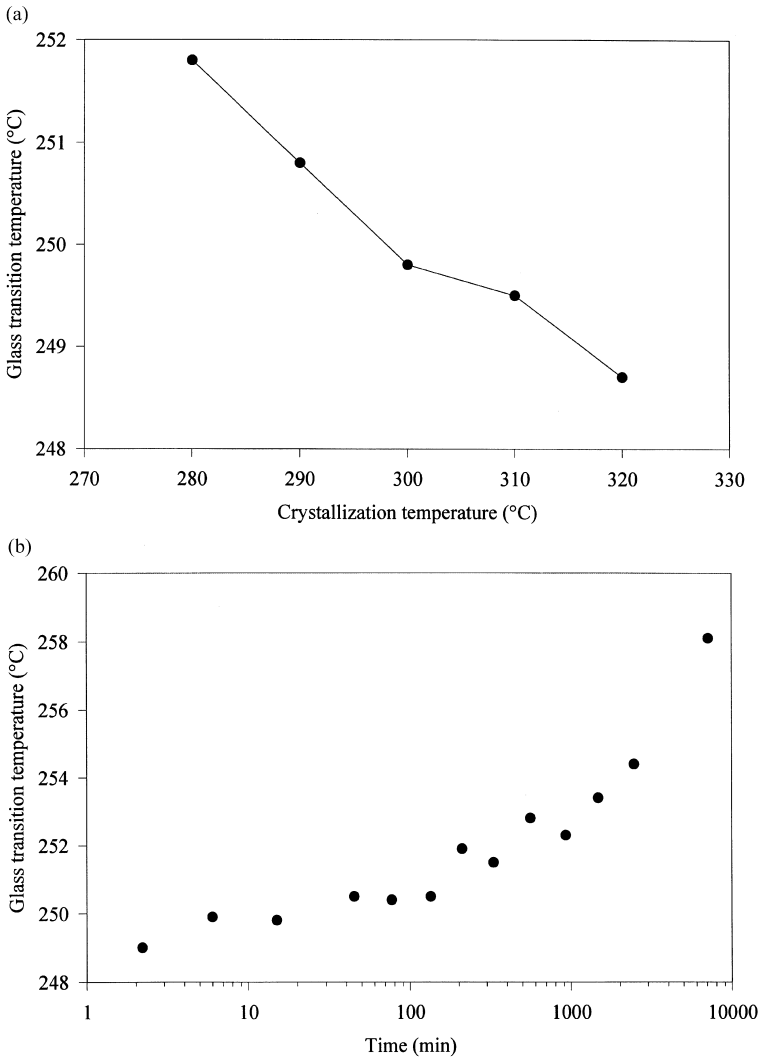

Figure 4 (a) Glass transition temperatures determined from d.s.c. as a function of crystallization temperature for crystallization times of 135 min. (b) Glass transition temperatures determined from d.s.c. as a function of crystallization time at a crystallization temperature of 300°C

time dependence of the degree of crystallinity from the WAXS studies.

Dynamic mechanical studies

We were unable to obtain a dynamic mechanical spectrum of a fully amorphous sample owing to the large extension of the sample in the instrument close to T_g. Therefore, the sample crystallized at 300°C for 2.2 min has been chosen as a 'representative amorphous sample'. Recall, however, that the d.s.c. and WAXS results discussed earlier showed that this sample indeed had a small fraction of crystallinity present. *Figure 5a* shows the storage modulus (E') as a function of temperature for a sample that had been crystallized at 300°C for 2.2 min. A prominent α relaxation is evident in the spectrum corresponding to the glass transition temperature. The storage modulus exhibits a dramatic decrease on going through the glass transition, this decrease being followed by an increase, which occurs as a result of cold-crystallization. *Figure 5b* shows the loss tangent of the same sample. The α relaxation is characterized by a sharp narrow tan δ peak, the position of which increases with increasing frequency. Interestingly, the magnitude of the α relaxation decreases with increasing frequency, suggesting thermorheological complexity, though it should be recognized that some crystallization could occur during the scan and hence influence the subsequent dispersion behaviour.

The dynamic mechanical data (E' and tan δ) for a semicrystalline sample which was crystallized at 300°C for 135 min is shown in *Figure 6a* and *b*. The figures clearly illustrate the effect crystallinity has on the α relaxation, in that the position of the tan δ peak is shifted by as much as 11°C to higher temperatures, indicating the constraining influence of the crystallites on the cooperative long-range amorphous chain motions that give rise to the glass transition. In contrast to the representative amorphous sample, the magnitude of the α relaxation peak increased with increasing frequency. Such behaviour has also been observed in dynamic mechanical relaxation studies on PEEK[44] and dielectric relaxation experiments on New TPI[24]. After the initial drop in storage modulus, there is a sudden change in the rate of decrease in modulus at *ca.* 315°C. This can be attributed to the melting of crystals corresponding to the lower melting endotherm ($T_c + 10$°C) that was observed in the same temperature range by d.s.c. studies as shown in *Figure 3*.

The peaks of the tan δ curves for samples that had been isothermally cold-crystallized at various temperatures for 135 min were higher by at least 8°C, compared with the representative amorphous sample. The magnitude of the

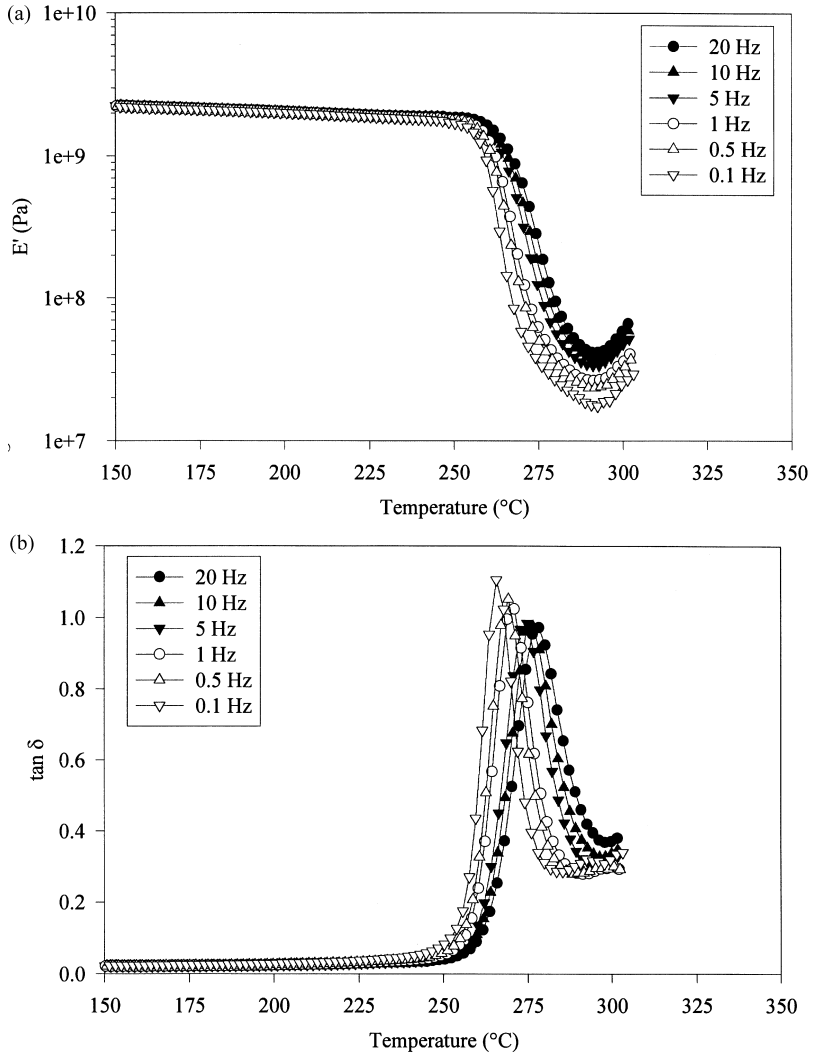

Figure 5 (a) Dynamic mechanical storage modulus for the representative amorphous sample (crystallized at 300°C for 2.2 min). (b) Dynamic mechanical loss factor for the representative amorphous sample (crystallized at 300°C for 2.2 min)

relaxation intensity was found to decrease with increasing crystallization temperature, this occurring due to an increase in the degree of crystallinity with increasing crystallization temperature, as was shown by the WAXS results discussed earlier. It was also observed that the position of the peak of the tan δ curve decreased with increasing crystallization temperature, which is consistent with the d.s.c. results shown in *Figure 4a*. Indeed, at a frequency of 1 Hz, the peak of the tan δ peak decreased by 3°C on increasing the crystallization temperature from 280°C to 320°C. This behaviour is not surprising in itself and has been previously reported by Cheng *et al.*[39] from their d.s.c. work on PEEK, Kalika *et al.*[44] from dynamic mechanical experiments on PEEK, and by Cebe *et al.*[25] from d.s.c. studies on New TPI. The glass transition temperature (peak of tan δ) decreases with increasing crystallization temperature in spite of an increase in the degree of crystallinity. This indicates that the relative constraint on the amorphous phase decreases with increasing isothermal crystallization temperature. An explanation offered by Cheng *et al.*[39] is that, at lower crystallization temperatures, crystallization occurs under more restrictive conditions, which gives rise to thinner and less perfect lamellae. This could increase the fraction of the amorphous phase that is associated with the crystal/amorphous interphase, accompanied by an increase in the strain at the interphase. The greater constraints on the amorphous phase could thus give rise to a higher and/or a broader glass transition behaviour than for the case of samples crystallized at higher temperatures, i.e. less restrictive conditions. Another explanation for this behaviour has been offered by Jonas *et al.*[45] who observed that for the case of PEEK, this decrease in the glass transition could be correlated with an increase in the thickness of the amorphous layer between lamellae. The difference between the study of Jonas *et al.*[45] and our study is the assignment of the amorphous layer thickness and crystal layer thickness from SAXS data, as discussed in the next section.

Under quiescent conditions of crystallization, semicrystalline polymers typically display a spherulitic superstructure. Each spherulite consists of outwardly radiating fibrils, which consist of stacks of chain folded lamellae, each lamella being separated from the other by an interlamellar amorphous layer. In the case of polymers displaying low degrees of crystallinity, the different lamellar stacks are also separated from each other by larger amorphous regions. For the case of polymers like PET and PEEK, this has been demonstrated among others by Lovinger at al.[46], Santa Cruz *et al.*[47] and Hsiao *et al.*[48]. This leads to the conclusion that in polymers displaying low

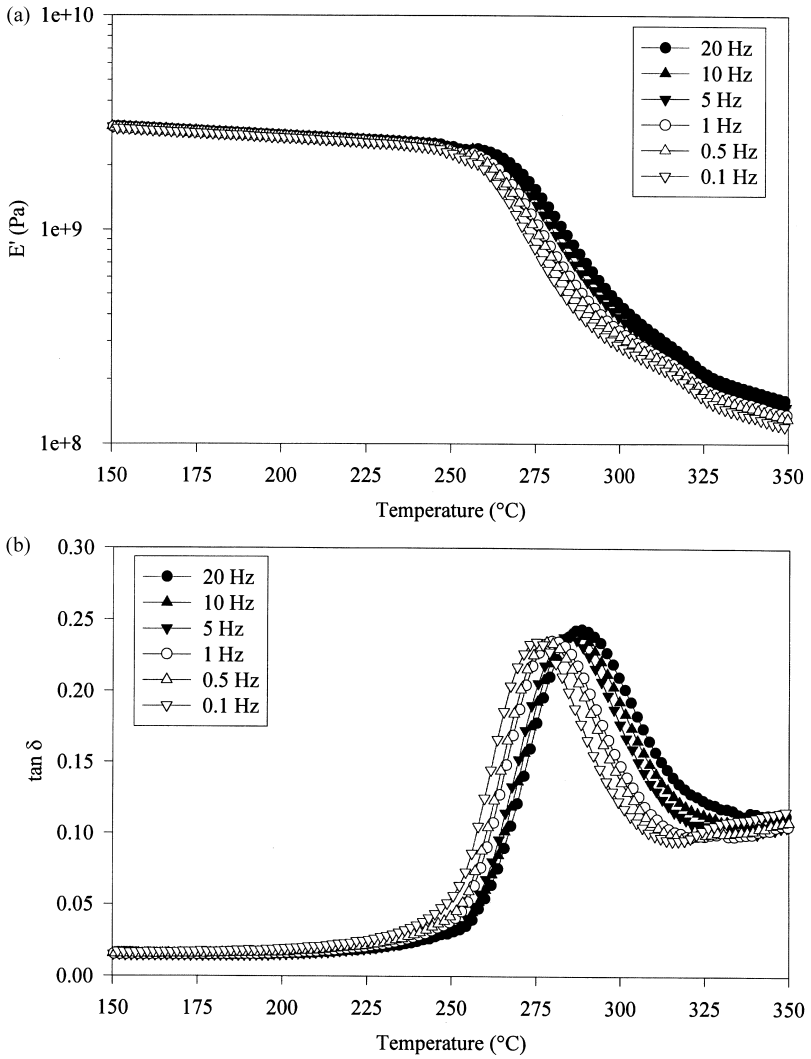

Figure 6 (a) Dynamic mechanical storage modulus for a sample crystallized at 300°C for 135 min. (b) Dynamic mechanical loss factor for a sample crystallized at 300°C for 135 min

degrees of crystallinity, we have two distinct amorphous regions. The inter-lamellar amorphous phase can be visualized as being more constrained than the amorphous regions between different lamellar stacks, which more closely resembles the free amorphous phase. If we were to believe that the inter-lamellar amorphous layers do not contribute significantly to the observed glass transition, the observed behaviour of the glass transition decrease with increasing crystallization temperature could be correlated with the size of the amorphous regions between different lamellar stacks and the number of constraints associated with these amorphous regions. However, if we were to assume that the inter-lamellar amorphous layers do indeed contribute to the glass transition, then the hypothesis of Jonas *et al*. as well as the explanation of Cheng *et al*. can be invoked to explain the decrease in glass transition with increasing crystallization temperature. As is described in more detail in the next section, the experimentally determined average amorphous layer thickness in our study increased from 47 Å to 56 Å as the crystallization temperature was increased from 280°C to 320°C. Since the repeat unit length of New TPI has been shown to be of the order of 25 Å[29], the amorphous layer thickness is approximately twice the repeat unit length. If the persistence length of New TPI is of the order of 50 Å, it would be difficult to visualize the inter-lamellar amorphous material greatly contributing to the observed glass transition. The observed decrease in the glass transition with increasing crystallization temperature would, in this case, arise mainly from the decreased constraints on the amorphous regions between lamellar stacks due to the presence of the crystallites. However, if the persistence length of New TPI is significantly smaller than 50 Å, then the inter-lamellar amorphous layer could also contribute to the observed glass transition. In this case, the decrease in the glass transition temperature with increasing crystallization temperature could occur due to both above reasons, i.e. increasing amorphous layer thickness as well as decreased constraints on the amorphous regions between different lamellar stacks.

Figure 7a shows the dynamic mechanical spectra (1 Hz) for a series of samples isothermally crystallized for various times at 300°C. Recall that the sample crystallized for 2.2 min is assumed to approximate the behaviour of an amorphous sample. The sample crystallized for 6 min shows a reduced relaxation intensity, an increase in the breadth of the relaxation peak, and an increase in the peak temperature indicating an increase in the glass transition temperature. The relaxation curve corresponding to a crystallization time of 45 min is further broadened and shifted to higher temperatures; the relaxation intensity is also reduced

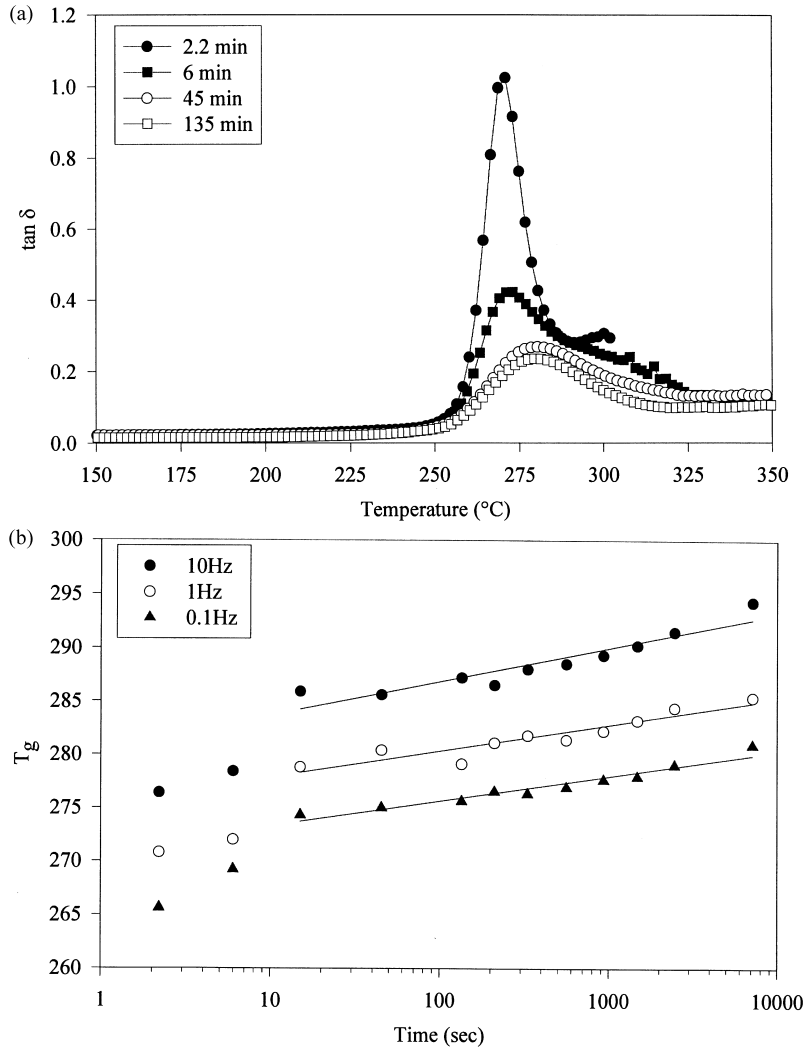

Figure 7 (a) Dynamic mechanical loss factor for samples crystallized at 300°C for various times. (b) Glass transition temperatures determined from the peak of tan δ as a function of crystallization time for samples crystallized at 300°C

compared with the sample crystallized for 6 min. The dynamic mechanical spectra of the samples crystallized for times higher than 45 min shift to higher temperatures and exhibit decreased relaxation intensities, but do not show any further broadening.

The increase in glass transition, as defined by the peak temperature in tan δ, with crystallization time is shown in *Figure 7b* for three frequencies, 0.1 Hz, 1 Hz and 10 Hz. As can be seen in the figure, for low crystallization times (2.2 min, 6 min), the glass transition temperature values fall significantly below the straight line fits obtained for the case of the higher crystallization times (>15 min). For times above 15 min, the glass transition displays a log time dependence on the crystallization (annealing) time. From d.s.c. cold-crystallization studies we know that the peak crystallization time (time required to reach the peak of the crystallization exotherm) is *ca.* 6 min. The peak crystallization time has generally been correlated with the time for spherulitic impingement in the sample. If we were therefore to assume that for crystallization times below 6 min, spherulitic impingement does not yet take place, then the morphology of the sample can be visualized as isolated spherulites dispersed in an amorphous matrix. Since the molecules remaining in the amorphous melt do not form part of any spherulite, they do not feel the constraints of crystallites, and therefore would be expected to display a lower glass transition than those molecules that are influenced by the presence of crystallites. For times greater than that required for impingement, all molecules in the amorphous phase would be influenced by the crystallites and would display higher glass transitions as well as a different dependence on crystallization time. Recall that the degree of crystallinity from WAXS measurements increased with the log of crystallization time; this increase in the degree of crystallinity would lead to an increase in the constraints on the amorphous phase. The increase in the glass transition temperature with the log of crystallization time can, therefore, be attributed to the increase in the constraints on the amorphous phase caused by lamellae that are formed as a result of secondary crystallization.

SAXS studies

The SAXS data for New TPI have been analysed using the correlation function approach of Vonk[49], and using the methods described by Strobl and Schneider[50] with reference to some of the terminology adopted by Santa Cruz *et al.*[47].

The correlation function is calculated from the Fourier–Bessel transform of the Lorentz corrected scattering profile. Before the Fourier transform can be carried out, the intensity has to be extrapolated to $q = 0$ and $q = \infty$, where q is the

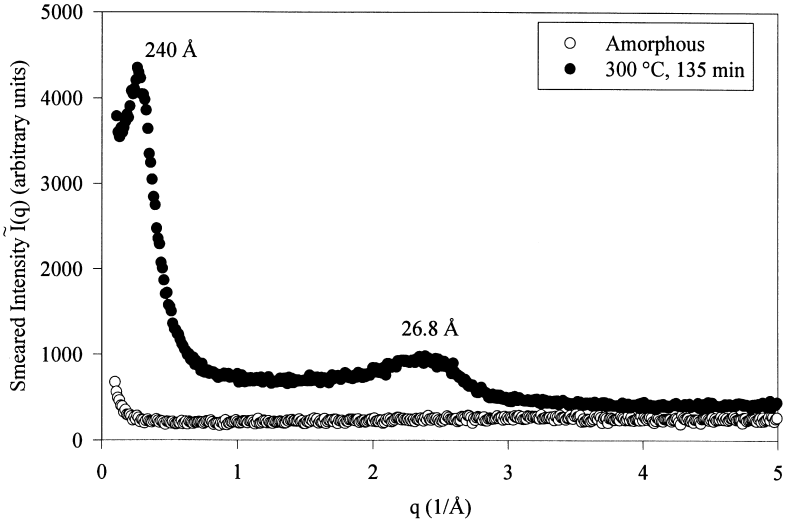

Figure 8 Smeared SAXS data for an amorphous sample and a semicrystalline sample

scattering vector defined as $q = 2\pi s$. The extrapolation to $q = 0$ was performed by an extrapolation between the first usable data point and the origin in the Lorentz corrected plot. The liquid scattering profile and the finite width of the crystal-amorphous interface were estimated using a modified form of Porod's Law[51], which was also used in the extrapolation of $q = \infty$.

The correlation function is then given by

$$\gamma(r) = \int_0^\infty [\tilde{I}(q) - I_b(q)]qe^{\sigma^2 q^2}\left[J_0(qr) - qrJ_1(qr)\right]dq \quad (4)$$

where $\tilde{I}(q)$ is the smeared intensity obtained from the Kratky measurement, J_0 and J_1 are Bessel functions of order 0 and 1 respectively. I_b is the background scattering arising from local electron density fluctuations, and σ is the standard deviation of a Gaussian distribution characterizing the phase boundary between the crystalline and amorphous regions. Since the correlation function has been normalized by the invariant, the value of the correlation function $\gamma(r)$ at the origin ($r = 0$) is 1.

The lamellar variables obtained from the data are the long period (L), the linear degree of crystallinity in the lamellar stacks (X_{cl}), the lamellar thickness (l_c) and the amorphous layer thickness (l_a). Using the terminology adopted by Santa Cruz *et al.*[47], we can determine two long periods from the correlation function: the position of the first maximum (L_c^M) and twice the value of the first minimum (L_c^m). The average linear degree of crystallinity in the lamellar stacks can be determined from the following equation

$$x_1 x_2 L_c^M = B \quad (5)$$

where B is the first intercept of $\gamma(r)$ with the abscissa, and x_1 and x_2 are the volume fractions of the two phases, respectively, in the lamellar stacks ($x_1 + x_2 = 1$). The assignment of either x_1 or x_2 to the crystalline phase is not so straightforward, however. There has been some controversy in the literature with regard to the assignment of x_1 and x_2 to the crystalline and interlamellar amorphous phases[51,52]. Regardless, the thicknesses of the two phases can be calculated by

$$l_1 = x_1 L_c^M \quad (6)$$

$$l_2 = x_2 L_c^M \quad (7)$$

Figure 8 shows the smeared SAXS profiles of a fully amorphous sample of New TPI and a semicrystalline sample that had been crystallized at 300°C for 135 min. The semicrystalline sample shows a prominent scattering peak at low angles corresponding to 240 Å, and a weaker scattering peak corresponding to *ca.* 27 Å. As discussed later in this section, the prominent scattering peak is a function of crystallization time and temperature, however, the weaker maxima was found to be independent of crystallization conditions. Recall that Okuyama *et al.*[29] had proposed a unit cell with $c = 25.11$ Å. The weaker maxima is thus believed to be due to the (001) reflection[22,23]. Note that the amorphous sample does not exhibit either a strong maxima or the weaker scattering peak corresponding to the (001) reflection. Cebe *et al.*[23] observed a weak scattering peak in their unrelaxed amorphous sample of New TPI processed film corresponding to a d-spacing of *ca.* 24 Å. This had been attributed by them to the (001) reflection. They explained this as being due to some amorphous phase orientation induced by the film processing operation. Similar effects have been noted earlier in the case of amorphous polyimide films subjected to tensile drawing, and attributed to lateral chain alignment[53], or described as smectic-like ordering[54]. The absence of the peak corresponding to the (001) reflection in our amorphous film strongly suggests that the samples used in this study did not possess any appreciable local range order that could give rise to a scattering peak.

Figure 9a shows the Lorentz corrected curves, as a function of the scattering vector q for a series of samples cold-crystallized for 135 min at different temperatures. From the figure it is obvious that as the cold crystallization temperature increases, the long spacing corresponding to the peak position of the scattering maximum (L_B) increases, i.e. the peak systematically shifts to lower values of q. *Figure 9b* shows the correlation functions of various samples whose intensity *versus* q curves are shown in *Figure 9a*. From the figure it is obvious that as the crystallization temperature increases, the long spacing increases to higher values of r. The value of L_c^M changed from 148 Å at a crystallization temperature of 280°C, to a value of 183 Å at a crystallization temperature of 320°C. The first intercept of the correlation function with the abscissa, B, also increases with increasing crystallization temperature as shown in *Figure 9b*. The value of the

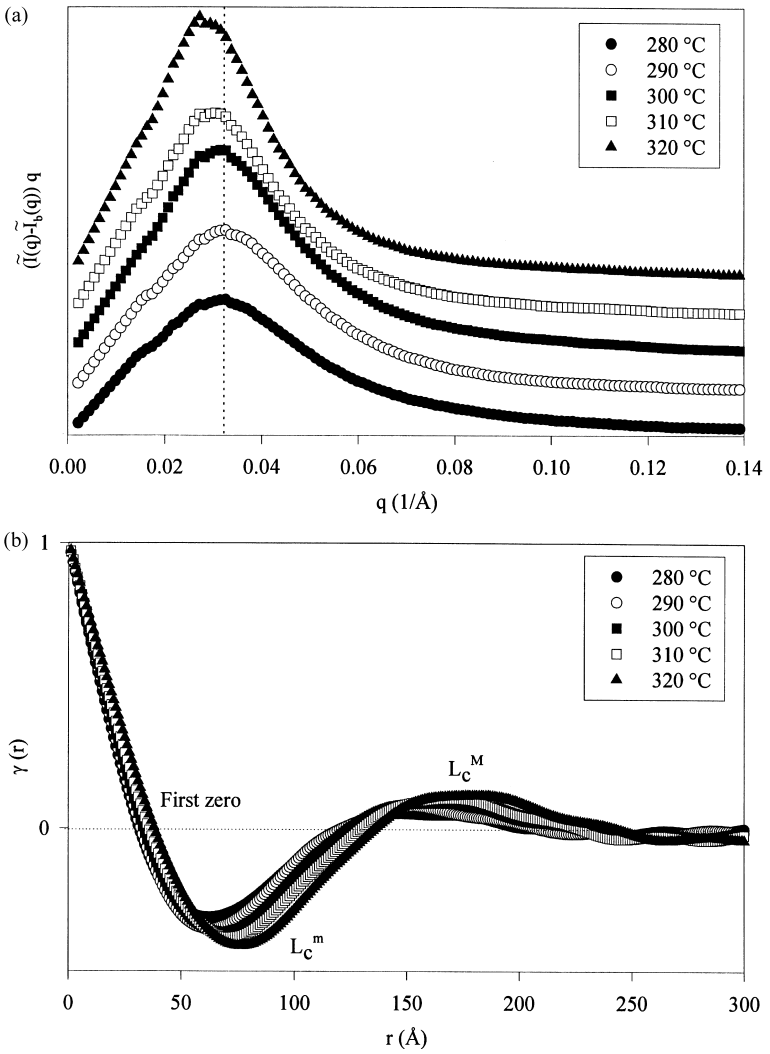

Figure 9 (a) Lorentz corrected plots for samples crystallized for 135 min at various temperatures. (b) Correlation functions for samples crystallized for 135 min at various temperatures

intercept was used in conjunction with the long spacing (L_c^M) in order to calculate the linear degree of crystallinity in the lamellar stacks; the values of x_1 and x_2 calculated from equation (5) yielded values of *ca.* 70% and 30%.

As mentioned earlier, there is no way a priori to assign these values to either the crystalline phase or the amorphous phase. Since the high angle weak reflection shown in *Figure 8* has been attributed to the (001) reflection, we can estimate the thickness of the lamella using the Scherrer analysis[33] on the width of the smeared (001) reflection. The Scherrer equation is given by

$$l_{hkl} = \frac{K\lambda}{\beta_o \cos\theta} \tag{8}$$

where l_{hkl} is the thickness in a direction perpendicular to the (*hkl*) plane, β_o is the breadth at half maximum of the (*hkl*) reflection in radians, K is a constant assumed to be unity, θ is half the radial scattering angle (2θ) corresponding to the maximum of the reflection, and λ is the wavelength of the X-ray used. Two points regarding our analysis must be emphasized; the first is that our line width analysis was carried out on raw data (smeared), and the second point is that this simple analysis ignores any effects of the presence of lattice defects, which could also cause line broadening. Nevertheless, our estimates of the lamellar thicknesses are shown in *Table 2* along with the lamellar thicknesses and amorphous layer thicknesses estimated from the correlation function, by assigning the thicker phase as the crystalline phase. It is obvious that the estimates from the Scherrer analysis are close to the lamellar thickness values obtained from the correlation function. A similar analysis was carried out by Hsiao *et al.*[22], who arrived at the same conclusion that the thicker phase value from the correlation function was close to the Scherrer analysis estimate. We have, therefore, assigned the larger value of l obtained from the correlation function to the lamellar phase. It should be mentioned here that the reverse assignment was made by Cebe *et al.*[25,27], whereas Hsiao[22] assigned the larger value to the lamellar phase, as we have.

Table 2 Average lammellar and amorphous layer thickness obtained from the correlation function and minimum lamellar thickness determined from Scherrer analysis

Crystallization temperature	l_c (Å)	l_a (Å)	l (Scherrer) (Å)
280°C	101	47	106
290°C	105	48	110
300°C	110	49	115
310°C	121	51	118
320°C	127	56	123

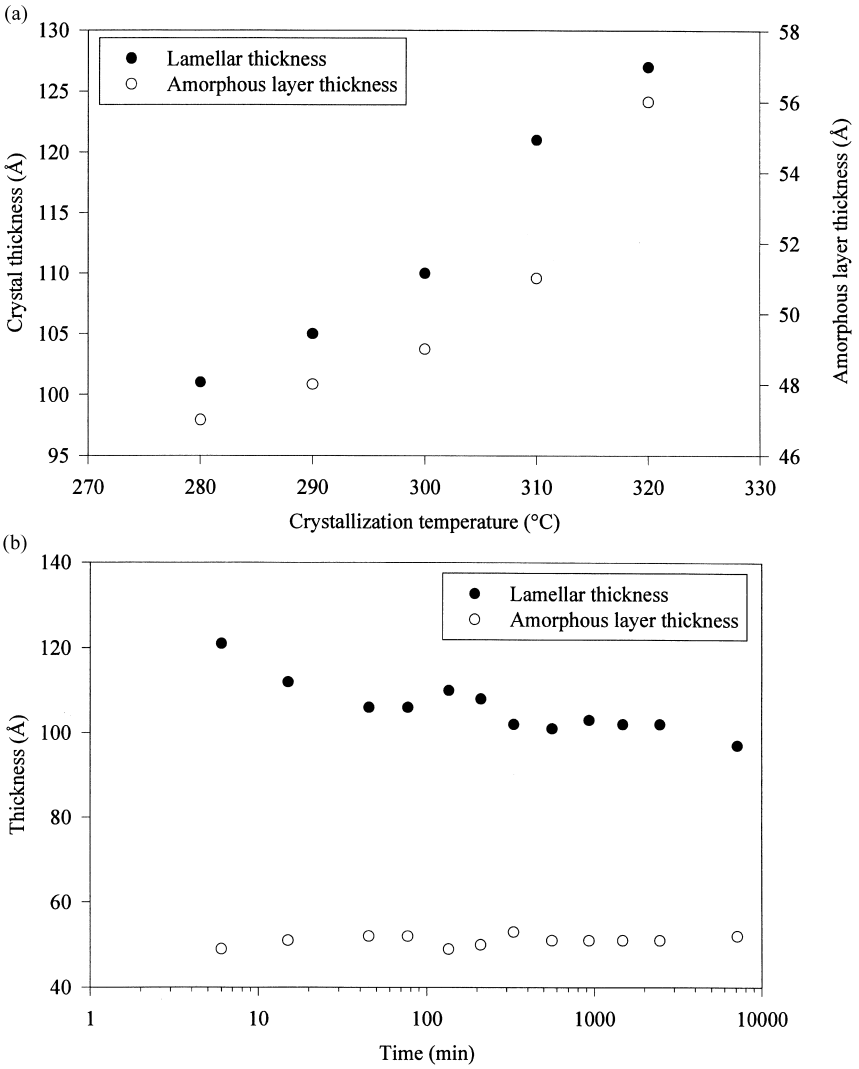

Figure 10 (a) Lamellar thickness and inter-lamellar amorphous layer thickness as a function of crystallization temperature for samples crystallized for 135 min. (b) Lamellar thickness and inter-lamellar amorphous layer thickness as a function of crystallization time for samples crystallized at 300°C

Figure 10a shows the change in lamellar thickness and amorphous layer thickness with crystallization temperature. It can be seen that both the lamellar thickness and the amorphous layer thickness increase with increasing crystallization temperature, with the lamellar thickness changing from 101 Å to 127 Å, and the amorphous layer thickness changing from 47 Å to 56 Å. Thus, we see that the increase in long spacing observed is due to an increase in both amorphous layer thickness and lamellar thickness. The increase in lamellar thickness with increasing crystallization temperature is to be expected on theoretical grounds since the thickness of a crystal formed at a lower undercooling ($T_m^\circ - T_c$) would be expected to be greater than a crystal grown at larger undercoolings. The increase in amorphous layer thickness with increasing crystallization temperature provides support for the explanation of Jonas *et al.*[44] regarding the dynamic mechanical results, which showed the glass transition temperature decrease with increasing crystallization temperature. Note, however, that the reverse assignment was made by Jonas *et al.*, i.e. the thicker phase was assigned to the amorphous phase and the thinner phase was assigned to be the lamellar thickness.

Figure 10b shows the lamellar thickness and amorphous layer thickness as a function of crystallization time. As can be seen from the figure, the amorphous layer thickness remains unchanged with crystallization time, however, the lamellar thickness decreases as a function of the log of the crystallization time. At the early stages of crystallization, primary lamellae are formed, the thickness of which is determined by the undercooling ($T_m^\circ - T_c$). At the end of the primary crystallization process, complete spherulitic impingement occurs, and the spherulites occupy the entire volume of the sample. There is, however, still a considerable fraction of amorphous material in the sample that could undergo crystallization. The WAXS results discussed earlier showed that a considerable fraction of the final crystallinity is generated during the secondary crystallization stage. Recall from our earlier discussion on the spherulitic morphology and our SAXS results presented here, that the lamellar stacks consist of bundles of lamellae separated by inter-lamellar amorphous layers of *ca.* 50 Å thickness. The rest of the amorphous phase is assumed to lie in larger amorphous regions between different lamellar stacks. The secondary crystallization process can continue in these amorphous regions, under more constrained conditions, following log time kinetics. These secondary lamellae are thinner than the lamellae formed during the primary crystallization process, and hence result in a net *decrease* in the average lamellar thickness detected by SAXS. This could lead to a bimodal distribution of lamellar thicknesses

in the system at the end of both primary and secondary crystallization processes, as has also been suggested earlier[51].

CONCLUSIONS

The crystallization, melting and relaxation behaviour of a commercial polyimide, Mitsui Toatsu's Aurum™ New TPI has been the focus of investigation in this study. Cold-crystallized samples with varying thermal histories were prepared in order to study the effect of crystallization history (time and temperature) on the structural, crystallization, melting and relaxation behaviour of this system. Since this polyimide has been the focus of considerable study over the recent years, a comprehensive picture of the crystallization behaviour has just begun to emerge.

It was found that the degree of crystallinity increased with increasing crystallization temperature, as evidenced by the WAXS results and a decrease in the relaxation intensity as shown by the dynamic mechanical results. Increasing the crystallization temperature also resulted in a decrease in the glass transition temperature observed both by d.s.c. and dynamic mechanical analysis. SAXS results showed that increasing crystallization temperature resulted in an increase in both lamellar and the inter-lamellar amorphous layer thicknesses. The decrease in T_g with increasing crystallization temperature is the result of a decrease in the number of constraints on the amorphous phase due to the presence of the crystallites. At this stage, we do not consider it very probable that the inter-lamellar amorphous regions greatly contribute to the observed glass transition, based on the fact that the inter-lamellar amorphous layer was of the order of 50 Å, which is *ca.* only twice the repeat unit length of New TPI. The glass transition is speculated to arise only from the amorphous regions between different lamellar stacks.

The effect of increasing crystallization time at 300°C was to increase the degree of crystallinity. This increase was prominent at low crystallization times, corresponding to a primary crystallization process, and was gradual, exhibiting log time kinetics at longer crystallization (annealing) times, due to secondary crystallization. A substantial fraction of the final crystallinity develops in this latter stage, as shown by the WAXS results, due to the formation of thinner lamellae in the amorphous regions between different lamellar stacks, as evidenced by a decrease in the average lamellar thickness observed by SAXS, causing the low endotherm observed in the d.s.c. heating scan. This is accompanied by greater constraints on the amorphous phase causing an increase in T_g as evidenced by the d.s.c. and dynamic mechanical results.

ACKNOWLEDGEMENTS

The authors would like to thank the NSF Science and Technology Center for High Performance Polymeric Adhesives and Composites for full funding of this study under contract number DMR 9120004. Useful discussions with Dr Ravi Verma regarding the SAXS and WAXS results is also acknowledged. We would like to thank Dr K. Blizard for donating the New TPI film used in this study.

REFERENCES

1. Feger, C. J., Khojasteh, M. M. and McGrath, J. E. ed., *Polyimides: Materials, Chemistry and Characterization*. Elsevier Science Publishers, Amsterdam, 1989.
2. Wilson, D., Stenzenberger, H. D. and Hergenrother, P. M. ed., *Polyimides*. Blackie, London, 1990.
3. Hergenrother, P. M., Heat Resistant Polymers in *Encycl. Polym. Sci. Eng*., Vol.7, 2nd edn. Wiley Interscience, New York, 1987, p. 639.
4. Mittal, K. L. ed., *Polyimides, Synthesis, Characterization and Applications*, Vol 1 and 2. Plenum Press, New York, 1984.
5. Muellerleile, J. T., Risch, B. G., Rodrigues, D. E. and Wilkes, G. L., *Polymer*, 1992, **34**, 789.
6. Brandom, D. K. and Wilkes, G. L., *Polymer*, 1994, **35**, 5672.
7. Brandom, D. K. and Wilkes, G. L., *Polymer*, 1995, **36**, 4083.
8. Srinivas, S., Graham, M., Brink, M. H., Gardner, S., Davis, R. M., McGrath, J. E. and Wilkes, G. L., *Polym. Eng. and Sci*, 1996, **36**, 1928.
9. Srinivas, S., Caputo, F. E., Graham, M., Gardner, S., Davis, R. M., McGrath, J. E. and Wilkes, G. L., *Macromolecules*, 1997, **30**, 1012.
10. Brink, M. H., Brandom, D. K., Wilkes, G. L. and McGrath, J. E., *Polymer*, 1994, **35**, 5018.
11. Rogers, M. E., Brink, M. H., Brennan, A. and McGrath, J. E., *Polymer*, 1993, **34**, 849.
12. Kim, Y. J., Glass, T. E., Lyle, G. D. and McGrath, J. E., *Macromolecules*, 1993, **26**, 1344.
13. Hergenrother, P. M., *Polymer Journal*, 1987, **19**, 73.
14. Hergenrother, P. M., Wakelyn, N. T. and Havens, S. J., *J. Polym. Sci., Polym. Chem. Ed.*, 1987, **25**, 1093.
15. Hergenrother, P. M. and Havens, S. J., *J. Polym. Sci., Polym. Chem. Ed.*, 1989, **27**, 1161.
16. Hergenrother, P. M., Beltz, M. W. and Havens, S. J., *J. Polym. Sci., Polym. Chem. Ed.*, 1991, **29**, 1483.
17. Havens, S. J. and Hergenrother, P. M., *J. Polym. Sci., Polym. Chem. Ed.*, 1992, **30**, 1209.
18. Heberer, D. P., Cheng, S. Z. D., Barley, J. S., Lien, H. S., Bryant, R. G. and Harris, F. W., *Macromolecules*, 1991, **24**, 1890.
19. Cheng, S. Z. D., Heberer, D. P., Lien, H. S. and Harris, F. W., *J. Polym. Sci.: Part B: Polym Phys.*, 1990, **28**, 655.
20. Kreuz, J. A., Hsiao, B. S., Renner, C. A. and Goff, D. L., *Macromolecules*, 1995, **28**, 6926.
21. Hsiao, B. S., Kreuz, J. A. and Cheng, S. Z. D., *Macromolecules*, 1996, **29**, 135.
22. Hsiao, B. S., Sauer, B. B. and Biswas, A., *J. Polym. Sci.: Part B: Polym. Phys.*, 1994, **32**, 737.
23. Friler, J. B. and Cebe, P., *Polym. Eng. and Sci.*, 1993, **33**, 587.
24. Huo, P. P. and Cebe, P., *Polymer*, 1993, **34**, 696.
25. Huo, P. P., Friler, J. B. and Cebe, P., *Polymer*, 1993, **34**, 4387.
26. Brillhart, M. V. and Cebe, P., *J. Polym. Sci.: Part B: Polym. Phys.*, 1995, **33**, 927.
27. Lu, S. X., Cebe, P. and Capel, M., *J. Appl. Polym. Sci.*, 1995, **57**, 1359.
28. Torre, L., Maffezzoli, A. and Kenny, J. M., *J. Appl. Polym. Sci.*, 1995, **56**, 985.
29. Okuyama, K., Sakaitani, H. and Arikawa, H., *Macromolecules*, 1992, **25**, 7261.
30. Hou, T. H. and Reddy, R. M., *SAMPE Q.*, 1991, January, 38.
31. Hirade, T., Hama, Y., Sasuga, T. and Seguchi, T., *Polymer*, 1991, **32**, 2499.
32. Mitsui Toatsu Chemicals Inc., Technical data sheet, Aurum™ Polyimide.
33. Alexander, L. E., *X-Ray Diffraction Methods in Polymer Science*. Wiley-Interscience, New York, 1969.
34. Ruland, W., *Acta Cryst.*, 1961, **14**, 1180.
35. Ruland, W., *Polymer*, 1964, **5**, 89.
36. Vonk, C. G., *J. Appl. Cryst.*, 1973, **6**, 148.
37. Verma, R. K., Srinivas, S., Wilkes, G. L. and Marand H., in preparation.
38. Wunderlich, B., *Macromolecular Physics*, Vol.3. Academic Press, New York, 1980.
39. Cheng, S. Z. D., Cao, M. Y. and Wunderlich, B., *Macromolecules*, 1986, **19**, 1868.
40. Cheng, S. Z. D., Wu, Z. Q. and Wunderlich, B., *Macromolecules*, 1987, **20**, 2802.
41. Chung, J. S. and Cebe, P., *Polymer*, 1992, **33**, 2312.
42. Chung, J. S. and Cebe, P., *Polymer*, 1992, **33**, 2325.
43. Velikov, V., Vivirito, J. and Marand, H., *Bull. Am. Phys. Soc.*, 1994, **39**(1), 168.
44. Krishnaswamy, R. K. and Kalika, D. S., *Polymer*, 1994, **35**, 1157.
45. Jonas, A. and Legras, R., *Macromolecules*, 1993, **26**, 813.
46. Lovinger, A. J., Hudson, S. D. and Davis, D. D., *Macromolecules*, 1992, **25**, 1752.
47. Santa-Cruz, C., Stribeck, N., Zachmann, H. G. and Baltá Calleja, F. J., *Macromolecules*, 1991, **24**, 5980.

48. Hsiao, B. S., Sauer, B. B., Verma, R. K., Zachmann, H. G., Seifert, S., Chu, S. B. and Harney, P., *Macromolecules*, 1995, **28**, 6931.
49. Vonk, C. G. and Kortleve, G., *Kolloid-Z.*, 1967, **220**, 19.
50. Strobl, G. R. and Schneider, M., *J. Polym. Sci. Polym. Phys. Ed.*, 1980, **18**, 1343.
51. Verma, R.K., Biswas, A., Marand, H. and Hsiao, B.S., *J. Appl. Crystallography*, in press.
52. Jonas, A. M., Russell, T. P. and Yoon, D. Y., *Macromolecules*, 1995, **28**, 8491.
53. Russell, T. P., Brown, H. R. and Grubb, D. T., *J. Polym. Sci. Polym. Phys. Ed.*, 1988, **25**, 1129.
54. Takahashi, N., Yoon, D. Y. and Parrish, W., *Macromolecules*, 1984, **17**, 2583.